Heat Transport Performance of Rotating Heat Pipes Installed in High-Speed Spindle

Ritsuo Hashimoto[*1] **Hikotaro Itani**[*1]
Keiji Mizuta[*1] **Kenji Kura**[*2]
Yasuro Takahashi[*3]

The correlations between the flow patterns of working fluid and the heat transport rates of the annular type heat pipes are compared through experiments and theoretical analysis. Consequently, both the critical rotational speeds for rimming or collapsing and those for transition of heat transport rates are shown to coincide each other and the simplified equations to estimate the critical speeds are shown. The analytical model to estimate the heat transfer efficiency at the rimmed condition is made using the Nusselt number got from experiments. Finally the heat pipe of 44 mm outer diameter is made and installed in the high-speed spindle motor and it is proved to decrease the temperature of the inner race of bearings from 70°C to 45°C at 24 000 rpm and successfully avoid the seizuring problem.

1. Introduction

The heat pipe transports the heat when the working fluid inside the pipe gets evaporated at the high-temperature zone and condensed at the low-temperature zone, ensuring higher heat transfer efficiency when the fluid circulation rate increases. The circulation power normally comes from the capillary force that uses the pressure difference between the gas phases and the wick in the liquid phase. However, the heat transfer efficiency can be further improved by making use of the centrifugal force when the pipe is rotated around the central shaft[(1)-(5)].

On the other hand, the rotary machine, such as a main spindle motor used in a machine tool for processing the work, has problems that with the increase in rotational speed the bearing gets overheated and causes seizure, and with the heat from the rotor added, the shaft undergoes thermal expansion, causing deterioration in working accuracy, etc. In order to avoid such problems, it is effective to cool down the revolving body from inside, and installation of heat pipe is the most effective means to this regard.

However, so far there is hardly any example of the heat pipe practically applied to this field, mainly because of the restriction of space for the installation of the heat pipe. Particularly the space at the center of the revolving shaft has to be left for the work and the jig to support it. This problem can be solved by using the concentric, double tube, i.e. the annular tube. However, such heat pipes have not yet been duly studied, and so far it is not possible to make the optimal design of the heat pipe to match with the given space and working conditions.

In this paper, the correlations between the flow patterns of the working fluid according to the rotational speeds of the heat pipes rotating round the horizontal shafts and the heat transport rates are compared through visualization experiment, then the heat transport rates at main pipe sizes are estimated through experimental and theoretical analysis, and finally the cooling effect when the heat pipe is installed to the motor is verified through experiments.

2. Flow pattern of liquid phase

The method of observation of the fluid flow pattern is shown in **Fig. 1**. A certain amount of fluid, fed into the gap of the acrylic pipe, is observed through the shaft end. The camera has its focus depth adjusted, and is set to a position where the slit light passes through the focus. The photo thus taken, is then subjected to picture processing, leaving only the green of the pipe and the outline of the fluid surface. In consideration of the fact that the shaft diameter of a main spindle motor is normally 30 to 80 mm and that the larger the diameter, the higher the output power, the inner diameter D of the outer barrel of the test pipe is set to be 74 mm. The working fluid used here is methanol methyl alcohol, which has effective vapor pressure for the temperatures 0 to 100°C the presumed temperature level of the revolving shaft of a motor.

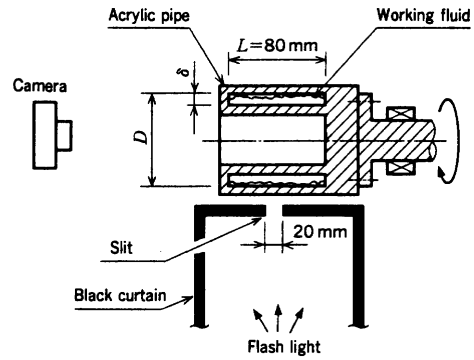

Fig. 1 Apparatus for visualization
The apparatus is designed to observe the circumferential liquid distribution in the center section of a revolving annular tube from the shaft end.

Fig. 2 shows the liquid distributions for various rotational speeds when the flow rate of the working fluid, charged into the 5.8 mm space of the annular tube, is taken as the flow rate for the total volume from the outer barrel to the inside, with the charged ratio ϕ_s being 0.045.

The arc angle of the outer barrel in the liquid pond at non-rotating state is about 77°C, with the top of the liquid coming in contact with the inner barrel. With the increase in rotational speed, the liquid gets lifted up in the direction of rotation, and when the rotational speed reaches the level 420 rpm (center left in the Fig.), the center of the liquid film rises to the position of approximately 60° from the tube bottom end, and the liquid surface becomes violently turbulent, causing the bubbles to get

*1 Hiroshima Research & Development Center, Technical Headquarters
*2 Hiroshima Machine Tool Works
*3 Hiroshima-Denki Institute of Technology

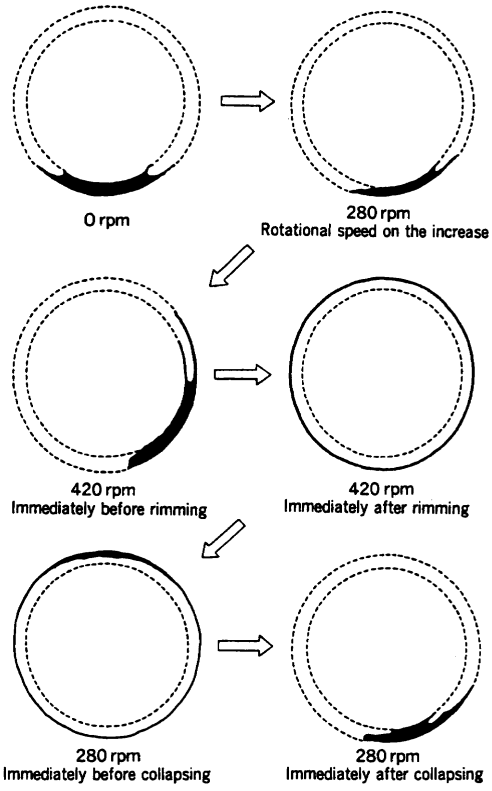

Fig. 2 Liquid distributions (liquid charged ratio ϕ_s: 0.045)

Changes in liquid distributions for various rotational speeds at the charged ratio of 0.045 is shown. The liquid film spreads at 420 rpm and collapses at 280 rpm.

rolled up and making the arc length at the liquid film pond longer. But the liquid is still in touch with the inner barrel. During the time this state is maintained, the liquid film spreads over the inner wall of the outer barrel, forming the rimming of the liquid film of uniform thickness. When the rotational speed is lowered down, the liquid film is found to have the film thickness increased at the top surface, leading to the collapsing of the film at 280 rpm. The liquid distribution after the collapsing is exactly the same as the distribution at the rotational speed before the rimming.

Fig. 3 shows the rotational speeds N_r and N_c for rimming and collapsing respectively when the charged ratio is ϕ_s changed. There is hardly any difference in N_r and N_c of each tube when the charged ratio is below 0.045. However, with the ϕ_s above the said level, the tube with smaller space δ is found to have lower N_r and N_c. Furthermore, N_r is found to have an extremely high value, with N_c being less dependent in ϕ_s than N_r.

The result of visualization test indicates that the angle to which the center of the liquid pond is lifted from the bottom end of the tube may be a clue condition for the formation of rimming. With the liquid shape immediately before rimming arranged in the form of a model as shown in Fig. 3, the relation between the charged ratio ϕ_s and angle of liquid film center from the bottom θ_r and the circumferential component W of the liquid specific gravity per unit shaft length can be approximately expressed by the equation given below by using the liquid density ρ, and gravitational acceleration g.

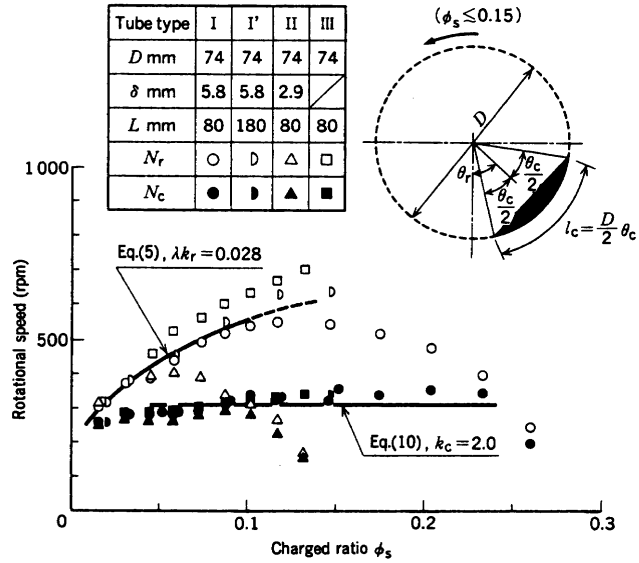

Fig. 3 Charged ratio ϕ_s and transitional rotation speeds N_r and N_c

Experimental values of charged ratio and transitional rotation speeds and the values using the approximate model equations when main dimensions of annular tube are changed.

$$W=\frac{\pi}{4}D^2\rho g\phi_s \sin\theta_r \tag{1}$$

Furthermore, the relation between the charged ratio and the arc angle θ_c of the liquid accumulated at the bottom can be approximately expressed as follows.

$$\phi_s=\frac{\theta_c^3}{12\pi} \quad (\theta_c \leqq 90°) \tag{2}$$

When this tube starts rotation, the shearing force F applied to the liquid from the annular tube causes the liquid in the liquid pond to get lifted to some angle. Supposing that the liquid is in touch only with the outer barrel, with the coefficient of friction of the flow being λ and the outer barrel inner circumferential velocity being v, the shearing force can be expressed as follows.

$$F=\lambda\frac{D}{2}\theta_c\frac{1}{2}\rho v^2 \tag{3}$$

In fact, however, the liquid pond immediately before rimming is extended towards the direction of rotation because of the liquid turbulence, causing θ_c to increase. Taking this into account and correcting θ_c with the coefficient k_r, and then substituting equation (2), equation (3) can be expressed as:

$$F=\lambda\frac{D}{2}k_r\theta_c\frac{1}{2}\rho v^2$$

$$=\lambda\frac{D}{2}k_r(12\pi\phi_s)^{1/3}\frac{1}{2}\rho v^2 \tag{4}$$

Supposing the rotational speed that balances W in equation (1) and F in equation (4) as the transitional rotation speed of rimming N_r, the N_r can be expressed as:

$$N_r=\left(\frac{1}{12\pi^4}\right)^{1/6}\left(\frac{g\sin\theta_r}{\lambda k_r}\right)^{1/2}\frac{\phi_s^{1/3}}{D^{1/2}} \tag{5}$$

In other words, N_r is proportional to ϕ_s to the 1/3 power. As for θ_r, it is clear from Fig. 2 that the rimming appears when the center of gravity of the liquid film is at about 60°. Furthermore, plotting the curve of equation (5) in Fig. 3 with λk_r = 0.028, there is an excellent coincidence with the experimental value

at $\theta_s < 0.15$. This indicates that the rimming for small θ_s can be expressed in terms of the relationship between the shearing force from the wall and the weight of the liquid.

The equation of motion of the liquid film in rimming state in circumferential direction can be expressed as follows by using the cylindrical coordinate that rotates with the tube at the angular velocity of ω.

$$\frac{\partial v}{\partial \tau}=\nu\frac{\partial^2 v}{\partial r^2}-g\sin(\omega\tau) \tag{6}$$

The distribution of the circumferential velocity appears in the direction of thickness of the liquid film due to the first item in the right hand side of equation (6), and the second item in the right hand side causes the distribution to become cyclical. When the momentum propagation depth inside the half-cycle is substantially smaller than the liquid film thickness, the first item in the right hand side of equation (6) can be ignored, so that:

$$\frac{\partial v}{\partial \tau}=-g\sin(\omega\tau) \tag{7}$$

Here, τ is the time. In other words, the liquid film gets synchronized with rotational cycle to cause oscillational flow. Taking into consideration that the average velocity of liquid film is equivalent to the peripheral velocity v_0 of the cylinder when $\omega\tau$ is supposed to be θ and $\theta = 0$ at the bottom end, and that the peripheral velocity of liquid film at the bottom end is maximum because the potential energy there is minimum, the equation (7) can be integrated with θ to obtain the equation as given below.

$$v=v_0+\frac{g}{\omega}\cos\theta \tag{8}$$

Since the flow rates are retained at each position of θ, the equation (8) can be expressed as follows by using the average flow velocity of liquid film v, film thickness δ and rotational speed N.

$$v\delta=\left(v_0+\frac{g}{\omega}\cos\theta\right)\delta=\text{Const}$$

$$\therefore\ \delta=\text{Const}\Big/\left(v_0+\frac{g}{\omega}\cos\theta\right)$$

$$=\text{Const}\Big/\left(\pi DN+\frac{g}{2\pi N}\cos\theta\right) \tag{9}$$

It can be expressed from the equation (9) that the film thickness δ becomes maximum when $\theta = \pi$, i.e. at the top end position, which corresponds with the result of visualization experiment. Furthermore, δ becomes infinite when the denominator in the right hand side is zero, giving rise to a jump phenomenon of fluid dynamics. In other words, the collapsing is considered to be attributed to the liquid film getting thick at the top due to the flow of the liquid film in circumferential direction. The rotational speed here can be expressed in the following manner.

$$N_c=k_c\frac{1}{\pi}\sqrt{\frac{g}{2D}} \tag{10}$$

According to the equation (10), the rotational speed N_c causing collapsing has nothing to do with the liquid film thickness or ϕ_s. This corresponds with Fig. 3, where the experiment values are uniform at ϕ_s between 0.03 and 0.23. The correction coefficient k_c is used as a multiplication factor in the equation (10) because the liquid film actually gets collapsed before δ becomes infinitely large. The results corresponds with the experimental results in Fig. 3 at $k_c = 2.0$.

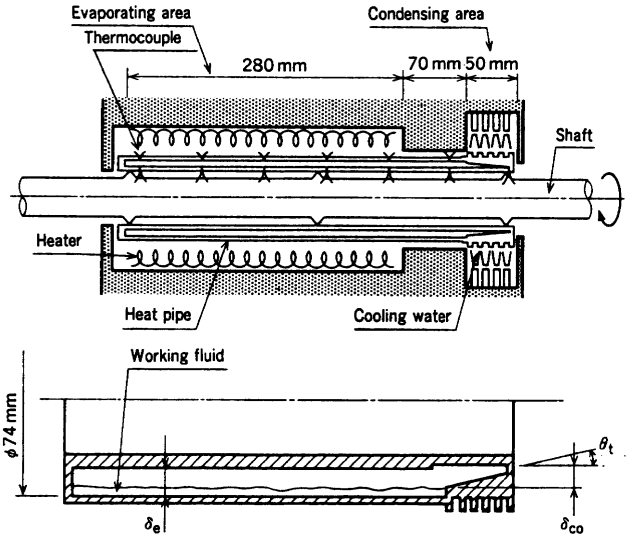

Fig. 4 Experimental apparatus of heat transport
Experimental apparatus for measuring the temperature distributions and heat transport rates of heat pipes is shown. The condensing surface of the heat pipe is tapered to improve the heat transfer efficiency.

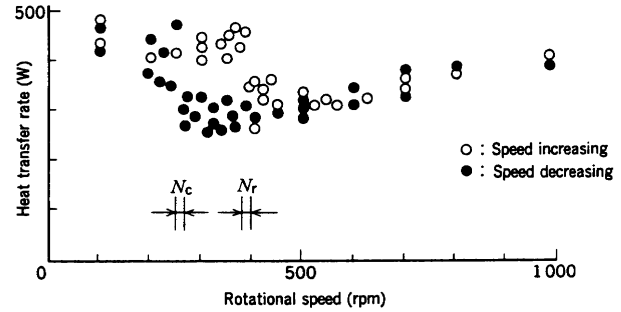

Fig. 5 Rotational speeds and heat transport rates
Heat transport rates for various rotational speeds, with charged ratio: 0.045 and annular space: 5.8 mm; undergoing changes at 400 rpm and 260 rpm.

3. Heat transport experiment

The experimental apparatus is shown in **Fig. 4**, where the heat pipe dimensions are set to match with the motor rotating shaft; inner diameter of the outer barrel: 74 mm, shaft length of the internal space: 400 mm. Here, the space of 280 mm at one side is considered as the evaporating area, and the 50 mm space at the end of the other side as the condensing area. The shaft in the condensing area is made shorter in length on the premise that the permissible space is small, and as a compensative measure, the condensing surface is tapered to contribute to a larger centrifugal force in order to promote the circulation of the liquid film. The inner diameter of the outer barrel in the evaporating area is made longer than that in the condensing area to form the stable liquid pond over the whole evaporating area. Methanol is used as the working fluid. The pipe is generally made of SUS 304 except for the outer barrel in the condensing area, which is made of copper. Fins are installed at the outer surface in order to reduce the thermal resistance in

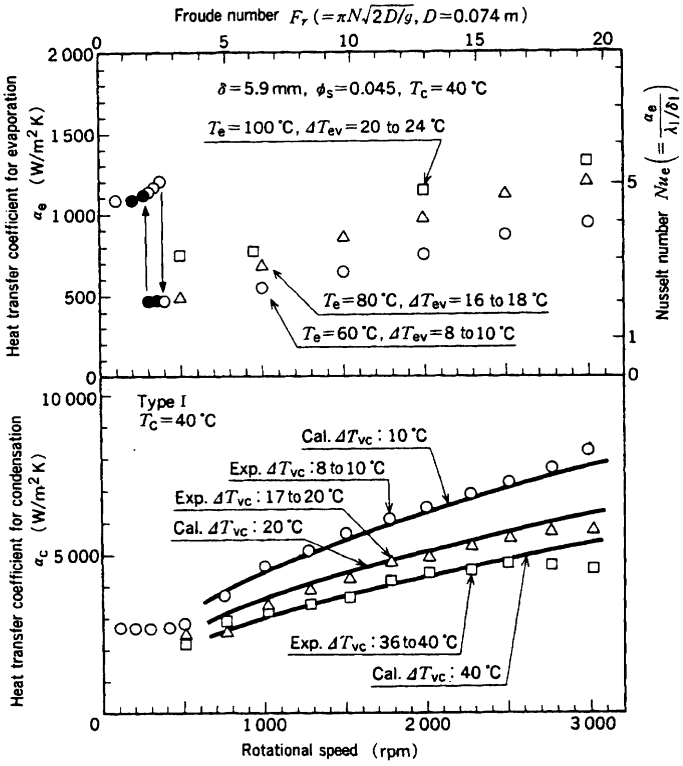

Fig. 6 Rotational speed, superheat temperature, and heat transfer coefficient for evaporation

Relationships between the rotational speeds, superheat degrees and the heat transfer coefficients for evaporation and condensation; the heat transfer coefficients on evaporating and condensing surfaces as the heat pipe rotational speeds are changed; with the heattransfer coefficients showing a rise when the rotational speed and superheat temperature on the wall surface are increased.

radial direction with a large heat flux. Thermocouples are installed to the inner and outer barrels to measure the pipe temperatures through slip rings.

The concentric cylindrical heater installed at the periphery of the evaporating area of the heat pipe is used for radiant heating from a close range, controlling the heater output to keep the temperature of the outer barrel in the evaporating area constant. In the condensing area, the fins at the outer surface are subjected to water cooling by means of the water applied horizontally from two sides. The temperature of the condensing surface is kept constant by adjusting the temperature and flow rate of the water. The temperatures and flow rates of the cooling water at the inlet and outlet are measured to obtain the heat transfer coefficiency.

Fig. 5 shows the measured data of the rotational speeds and heat transport rates of heat pipes, indicating the transitional phenomena of the heat transport rates getting sharply changed due to rotational speeds at the time of speed increasing and decreasing, with rimming and collapsing taking place at rotational speeds 400 rpm and 270 rpm respectively. The results almost conform to the transitional rotation speeds at the charged ratio ϕ_s = 0.045 in Fig. 3. It can, therefore, be deduced that the transition of heat transport rate due to rotational speed is attributed to the transition in the fluid form of the working fluid.

Fig. 6 shows at the top the relationship between the rotational speed and superheat degree mainly at rimming state and the heat transfer coefficient for evaporation in the evaporating area. The rotational speed here is made non-dimensional, and is expressed in Froude number by the equation given below.

$$F_r=\pi N\sqrt{\frac{2D}{g}} \tag{11}$$

As for the vapor temperature, the almost equivalent temperature inside the inner barrel is adopted, with T_e and T_c being respectively the temperatures of evaporating surface and condensing surface, while ΔT_{ev} the temperature difference between evaporating surface and vapor. The vertical axis at the right hand side expresses the Nusselt number with the liquid film thickness as the representative length. The graph shows that the heat transfer coefficient for evaporation increases when the rotational speed and superheat degree are increased. Moreover, since the Nusselt number is larger than 1, the liquid film is considered to get evaporated due to boiling or natural convection. The relationship between the rotational speed and superheat degree and the heat transfer coefficient for condensation in the condensing area is plotted at the bottom of Fig. 6, where ΔT_{vc} is the temperature difference between vapor and condensing area. The heat transfer coefficient for condensation also rises when the superheat degree and rotational speed are increased. These relationships will be theoretically analyzed in the following section.

4. Analysis of heat transport rate

Experimentally the condensed liquid film in a heat pipe is in the state of laminar flow, with its thickness becoming the dominant thermal resistance. The relation between the film thickness δ and the liquid film flow rate V_l at that position can be expressed in the following manner, where ν_l is the Kinematic viscosity of the liquid film, r the radius of the condensing surface, ω the angular velocityof rotation, θ_t the taper angle and $d\delta/dx$ the gradient of the film thickness.

$$\left.\begin{aligned} V_l&=\frac{2}{3}c_l\pi r\delta^3 \\ c_l&=\frac{r}{\nu_l}\omega^2\left(\cos\theta_t\frac{d\delta}{dx}-\sin\theta_t\right)\end{aligned}\right\} \tag{12}$$

Furthermore, the condensation flow rate can be expressed by using the latent heat for condensation ΔH, coefficient of thermal conductivity of liquid film λ_l, vapor temperature T_v and temperature T_c at the condensing surface in the following manner.

$$\left.\begin{aligned} \frac{dV_l}{dx}&=2\pi r\frac{q_c}{\Delta H\,\rho_l} \\ q_c&=\lambda_l(T_v-T_c)\delta\end{aligned}\right\} \tag{13}$$

By coupling the above two equations (12) and (13), and by supposing that the liquid flow rate at the shaft end is zero, it is possible to obtain the distribution of liquid film thickness in x direction, the profile of condensing heat flux and the overall heat transfer coefficient for condensation. The results of analysis are shown in full lines at the bottom of Fig. 6. The analytical data, expressed in full lines, show conformity to the experimental data at rotational speeds over 800 rpm, with the difference within 10%, verifying the validity of the analysis model.

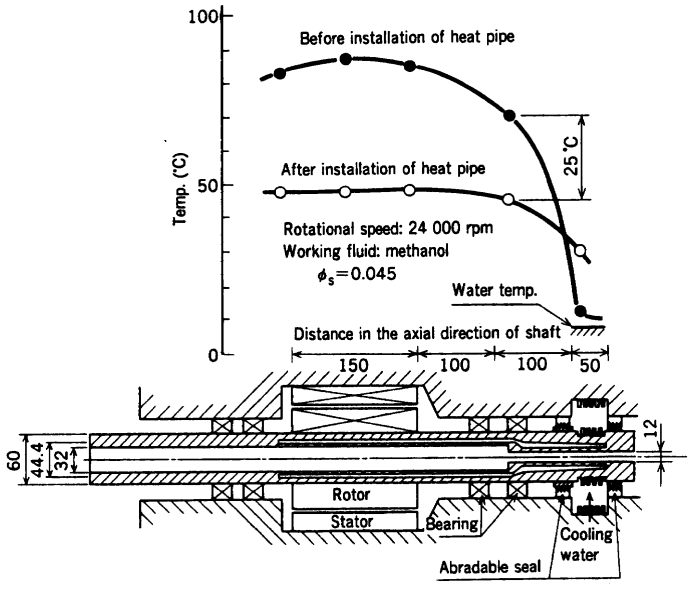

Fig. 7 Temperature profiles of motor shaft
Temperature profiles of motor shaft before and after installing the heat pipe to the motor shaft; the temperature at the bearing after installing the heat pipe is 25°C less than that before installing.

5. Cooling effect on motor shaft

With the heat transport performance of the rotating heat pipe made clear, the heat pipe is installed to the rotating motor shaft to verify the cooling performance. **Fig. 7** shows the main dimensions of motor shaft and heat pipe, and the temperature distribution on the outer surface of rotating motor shaft. The cooling section has fins installed to be water cooled externally. The cooling water is sealed against the bearing by attaching abradable seals on both sides of the cooling section. The temperature distribution here is for the rotational speed of 24 000 rpm. The bearing temperature is found to be lowered from 70°C to 45°C due to the effect of the installation of heat pipe.

6. Conclusion

The following achievements have been made through the elementary tests on the annular type rotating heat pipe and the verification tests made after installing the heat pipe to the motor shaft.

(1) The flow patterns of the liquid phase of working fluid and the transitional limit of the heat transport rate against the rotational speed have been experimentally made clear, and their approximate equations have been deduced.
(2) It has been verified that the heat transport rate of the heat pipe can be analytically estimated through comparison with the experimental data.
(3) It has been verified that the heat pipe, when installed to the motor shaft, shows the cooling effect by lowering the bearing temperature from the conventional level of 70°C to 45°C.

References

(1) Nimmo, B. G. and Leppert, G., Heat Transfer 1970, 6 (1970) Elserier Pub.
(2) Marto, P. J. and Wagenseil, AIAA J., 17-6 (1979) p.647
(3) Daniels, T. C. and Al-Jumaily, F. K., I. J. Heat Mass Transfer, Vol.22 (1979) p.1 237—1 241
(4) Katsuta, M., Kigami, H., et al., Proc. 5th IHPC (1984) p.126—132
(5) Nakayama, W., Ohtsuka, Y. and Yoshioka, T., Proc. 5th IHPC (1984) p.121—125